

EVOLUTION OF THE 1919 EJECTA OF V605 AQUILAE^{*,†}

GEOFFREY C. CLAYTON¹, HOWARD E. BOND^{2,3,4}, LINDSEY A. LONG⁵, PAUL I. MEYER⁵, BEN E. K. SUGERMAN⁵, EDWARD MONTIEL¹, WILLIAM B. SPARKS², M. G. MEAKES², O. CHESNEAU⁶, AND O. DE MARCO⁷

Draft version August 20, 2019

ABSTRACT

New imaging of V605 Aql, was obtained in 2009 with *HST*/WFPC2, which had a nova-like outburst in 1919, and is located at the center of the planetary nebula (PN), Abell 58. This event has long been ascribed to a final helium shell flash, but it has been suggested recently that it may instead have been an ONe nova. The new images provide an 18 year baseline for the expansion of the ejecta from the 1919 event. In addition, the central star has been directly detected in the visible for the first time since 1923, when it faded from sight due to obscuration by dust. The expansion of the ejecta has a velocity of ~ 200 km s⁻¹, and an angular expansion rate of ~ 10 mas yr⁻¹, consistent with a 1919 ejection. This implies a geometric distance of 4.6 kpc for V605 Aql, consistent with previous estimates. The gas mass in the central knot of ejecta was previously estimated to be $5 \times 10^{-5} M_{\odot}$. It is estimated that warm dust associated with this gas has a mass of $\sim 10^{-5} M_{\odot}$. There is also evidence for a significant amount, $10^{-3} M_{\odot}$, of cold (75 K) dust, which may be associated with its PN. The knot ejected in 1919 is asymmetrical and is approximately aligned with the asymmetry of the surrounding PN. Polarimetric imaging was obtained to investigate whether the 2001 spectrum of V605 Aql was obtained primarily in scattered light from dust in the central knot, but the signal-to-noise in the data was insufficient to measure the level of polarization.

Subject headings: stars: individual (V605 Aql)

1. INTRODUCTION

In the second decade of the 20th century, the variable star V605 Aquilae underwent a remarkable outburst (Clayton & De Marco 1997; Clayton et al. 2006). Its eruption was discovered by Wolf (1920) on plates taken at Heidelberg, with the star reaching a maximum photographic magnitude of 10.2 in 1919 August. Subsequent investigation of Harvard plates by Ida Woods showed that V605 Aql had slowly risen to its maximum over the previous 2 years (Bailey 1921). The historical visual and photographic photometry has been assem-

bled and discussed by Duerbeck (2002, see also Harrison (1996)). Although initially considered to be a very slow nova—it was designated Nova Aquilae No. 4—V605 Aql had a light curve unlike that of any known nova. After fading in 1920, it re-brightened in 1921, faded again, and then brightened yet again in 1923, before finally fading from sight. Fuhrmann (1981) examined over 400 plates obtained between 1928 and 1979, and found that V605 Aql was always below photographic magnitude, 16–17.5, during this interval. Spectroscopy obtained in 1921 September, showed the object to be a cool carbon star, with a spectral type of R0, in stark contrast to the high-excitation emission-line spectra of classical novae at late outburst stages (Lundmark 1921).

In spite of these unique features, V605 Aql was almost entirely ignored by astronomers over the ensuing five decades. Modern interest was rekindled by Bidelman (1971), who reviewed the scanty data and made the novel suggestion that V605 Aql had been an extragalactic supernova (SN). His speculation was based on Lundmark’s R0 classification along with the fact that the first SN whose spectrum was photographed, Z Centauri (SN 1895B), had a spectrum that had been considered to resemble that of an R-type star by Cannon & Pickering (1916). However, Bidelman (1973) subsequently was able to examine Lundmark’s original 1921 spectrograms, and verified that V605 Aql in outburst indeed was a carbon star—in fact, a *hydrogen-deficient* carbon (HdC) star, closely similar to the well-known non-variable HdC star HD 182040, as well as other cool R Coronae Borealis (RCB) stars (Clayton 2012). The 1921 spectrum was re-examined and presented in Clayton & De Marco (1997).

Following up on Bidelman (1971), van den Bergh (1971) obtained deep photographs of V605 Aql with the 5-m Hale telescope. These images showed it to be the

¹ Dept. of Physics & Astronomy, Louisiana State University, Baton Rouge, LA 70803; gclayton@fenway.phys.lsu.edu, emonti2@lsu.edu

² Space Telescope Science Institute; 3700 San Martin Drive, Baltimore, MD 21218; bond, sparks@stsci.edu, mgmeakes@gmail.com

³ Department of Astronomy & Astrophysics, Pennsylvania State University, University Park, PA 16802

⁴ Current address: 9615 Labrador Ln., Cockeysville, MD 21030

⁵ Dept. of Physics and Astronomy, Goucher College, 1021 Dulaney Valley Rd., Baltimore, MD 21204; ben.sugerman@goucher.edu

⁶ Observatoire de la Côte d’Azur-CNRS-UMR 6203, Dept Gemini, Avenue Copernic, F-06130 Grasse, France; olivier.chesneau@ob-azur.fr

⁷ Dept. of Physics, Macquarie University, Sydney, NSW 2109, Australia; orsola@science.mq.edu.au

⁸ European Southern Observatory, Karl-Schwarzschild-Strasse 2 D-85748 Garching bei München, Germany; fkerber@eso.org

* Based on observations made with the NASA/ESA *Hubble Space Telescope*, obtained by the Space Telescope Science Institute, and from the data archive at STScI. STScI is operated by the Association of Universities for Research in Astronomy, Inc., under NASA contract NAS5-26555.

† We dedicate this paper to the memories of William P. Bidelman (1918–2011) and Martha L. Hazen (1931–2007)—teachers, colleagues, friends, lovers of the stars.

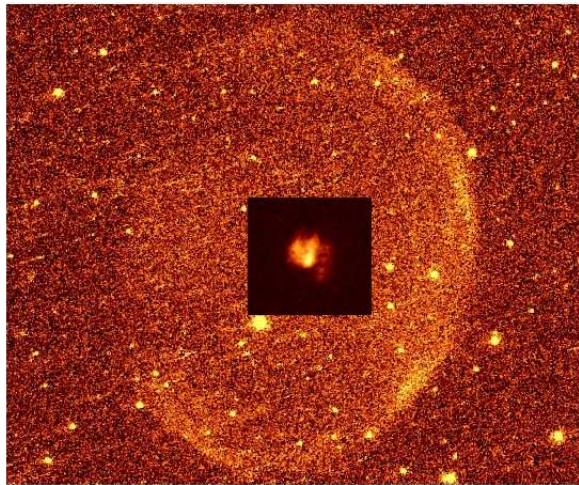


FIG. 1.— Combined F658N ([N II]) *HST* WFPC2 image from the Hubble Legacy Archive with an inset showing a magnified image of the central knot. The relative orientations of the inner knot and the outer PN are similar. North is up and East is to the left and the size of the image is approximately $50'' \times 50''$. The inset is $5'' \times 5''$.

central star of a large, very faint, old planetary nebula (PN), which had already been cataloged as object 58 in the Abell (1966) list of faint PNe discovered in the course of the Palomar Observatory Sky Survey (POSS). Abell 58 (PN G037.5–05.1) has an elliptical shape, with dimensions of $44'' \times 36''$. See Figure 1.

Based on these findings—a cool, hydrogen-deficient star erupting in the center of an old PN—many investigators believe V605 Aql to be a star that underwent a final helium-shell flash (FF), an event first described theoretically by Iben et al. (1983). In the FF scenario, a hot PN nucleus (PNN) re-ignites He shell burning, retraces its evolution to become temporarily a “born-again” red giant whose remaining surface hydrogen has been ingested and burned, and then evolves back to its original high surface temperature. Recent theoretical models indicate that the transition from a hot PNN to a cool giant, and then back again, can occur in as little as 5–10 yr. Such extremely rapid evolution results from a very late thermal pulse, in which the star experiences a FF only when it has already reached the top of the white-dwarf cooling track with a very thin envelope remaining (Herwig 2001; Lawlor & MacDonald 2003; Hajduk et al. 2005).

V605 Aql in 1921 had a spectrum resembling that of a cool RGB star with $T_{\text{eff}} \simeq 5000$ K (Clayton & De Marco 1997). However, there is evidence that it had reheated no later than the mid-1970s, and likely as early as the early 1950s, if not even earlier. At present, a dusty knot of extremely hydrogen-deficient nebulosity, unresolved or marginally resolved in ground-based optical images, lies at the site of V605 Aql at the center of the large, faint PN, Abell 58 (Clayton & De Marco 1997; Clayton et al. 2006). The spectrum of the compact knot is extraordinary. It shows strong emission lines of [O III], but no sign of the Balmer lines (Seitter 1985). The surrounding PN, however, has a fairly normal hydrogen-rich composition (e.g., Ford 1971; Wesson et al. 2008). Optical spectra of the knot, obtained in 2001, confirm the presence of broad, high-excitation Wolf-Rayet stellar features, including strong C IV emission, and clearly demonstrate

that the star is again very hot, $\sim 95,000$ K (Clayton et al. 2006). Since the knot is visible in blue POSS images obtained in 1951, V605 Aql was most likely already producing ionizing radiation and strong [O III] emission by that time. A spectrogram obtained in the mid-1970s by P. Osmer with the Cerro Tololo 4-m telescope at the request of H.E.B. showed the nebular emission lines, but unfortunately the unpublished data have now been lost. The compact knot is probably material ejected in the 1919 outburst, which is so dusty that it hides the star from direct view; possibly we see only starlight that emerges after scattering off the dust (Clayton et al. 2006).

The behavior of V605 Aql is very similar to that seen more recently in Sakurai’s Object (V4334 Sgr), which also lies within a very faint PN. After a rapid brightening in 1996, followed by several fluctuations, Sakurai’s Object went into a deep decline in 1999, just as V605 Aql did in 1923 (Kerber et al. 1999; Duerbeck 2002). Thick dust formed around both stars, causing their precipitous optical declines. The spectrum of Sakurai’s Object in 1997 was very similar to the 1921 spectrum of V605 Aql (Kerber 2001). Also, Sakurai’s Object shows evidence for new circumstellar ionized gas only 10 years after its outburst (Kerber et al. 2002; Hajduk et al. 2005), suggesting that it is already becoming hot again. Thus, the current behavior of V605 Aql is a template for the future behavior of Sakurai’s Object. Another FF object, also surrounded by an old PN, FG Sge, is evolving much more slowly than the near-twins V605 Aql and Sakurai’s Object (Duerbeck 2002; Lechner & Kimeswenger 2004).

Recently, however, the FF scenario for V605 Aql has been questioned by Wesson et al. (2008) and Lau et al. (2011). They carried out a spectroscopic analysis of the V605 Aql central knot, showing a C/O ratio below unity and an remarkably high abundance of Ne, properties that are in stark conflict with theoretical models of FF events. These findings suggest a more complicated evolutionary history, involving a ONe white dwarf involved either in a binary merger or in an unusual classical-nova outburst.

In this paper, we present new polarimetric high-resolution imaging of V605 Aql with the *Hubble Space Telescope* (*HST*). The polarimetry was done to investigate whether the recent spectrum of V605 Aql is seen only in scattered light, in which case the knot surrounding the star should be highly polarized. These new images also provide an 18 year baseline to measure the expansion and evolution of the central knot. We examine the morphology and angular expansion of the compact nebula, estimate its distance and reddening, while discussing the implications for the nature of V605 Aql.

2. OBSERVATIONS AND DATA REDUCTION

2.1. *HST*

V605 Aql has been imaged at three epochs by *HST*, as summarized in Table 1. Observations were made at epoch 1991.60 (PI: H.E.B.) with the aberrated Faint Object Camera (FOC) at $f/96$ in two broad-band ultraviolet filters, an optical blue continuum filter (F437M), and a narrow-band filter isolating [O III] 5007 Å. The compact nebula was detected only in the [O III] exposure, listed in Table 1. Brief discussions of the 1991 images were given by Bond et al. (1992, 1993) and Bond & Pollacco (2002), and the images were described

TABLE 1
HST IMAGING OF V605 AQUILAE USED IN THIS STUDY

Date [UT]	Instrument	Filter	Image Scale [''/pix]	Exposure [s]	Program ID/PI
1991 Aug 6	FOC	[O III] F501N	0.014	796	2570/Bond
2001 May 27	WFPC2/WF3	[O III] F502N	0.100	1050	9092/Hinkle
2001 May 27	WFPC2/WF3	[N II] F658N	0.100	460	9092/Hinkle
2009 Mar 9	WFPC2/PC	[O III] F502N	0.046	800	11985/Clayton
2009 Mar 9	WFPC2/PC	[N II] F658N	0.046	1200	11985/Clayton
2009 Apr 3-5	WFPC2/WF2	C IV F547M + polarizers	0.100	12,600	11985/Clayton

in more detail by Clayton & De Marco (1997). Second-epoch observations were obtained at 2001.40 (PI: K. Hinkle) using the Wide-Field 3 chip (WF3) of the Wide Field Planetary Camera 2 (WFPC2) and filters isolating [O III] 5007 Å and [N II] 6583 Å. Details of these observations are given by Hinkle et al. (2008), who also presented high-resolution ground-based near-IR images.

The new third-epoch imaging, reported here, were obtained at epoch 2009.21 (PI: G.C.C.). Narrow-band WFPC2 frames in the nebular [O III] 5007 Å and [N II] 6583 Å emission lines were obtained with the PC1 chip, making these the highest-resolution optical images available for V605 Aql.

We also used WFPC2 to obtain polarimetric images at epoch 2009.3 in the medium-band F547M filter, which in the case of V605 Aql transmits the broad Wolf-Rayet C IV 5806 Å band emitted in the wind of the central star, and mostly rejects emission from the surrounding nebula. Thus the F547M signal is expected to be dominated by direct light from the central star, plus any component of starlight scattered by the surrounding dust before emerging from the compact nebula, which would be expected to be linearly polarized.

For the polarimetric imaging, we used “Strategy 2c,” as outlined by Biretta & Sparks (1995). The technique is to place the target in a corner of the WF2 chip near the amplifiers (for less degradation by charge-transfer inefficiency in the aging detector) and make exposures with four polarizer rotations, denoted POLQ, POLQP15, POLQN33, and POLQN18. These yield respective electric-vector orientations of 0°, 15°, 102°, and 117°, relative to the telescope orientation angle. The exposures were made during three two-orbit visits, accumulating totals of 3100 or 3200 s in each of the four polarizer settings.

Pipeline-calibrated *HST* images were retrieved from the archive and processed as follows: (1) The 1991 FOC [O III] image, obtained with the aberrated telescope, was deconvolved using 80 iterations of the Lucy-Richardson procedure in the IRAF/STSDAS¹¹ package. Pictorial representations of the raw and deconvolved images have been presented by Bond & Pollacco (2002). (2) The

WFPC2 images from 2001 and 2009 were combined using *multidrizzle* (within the STSDAS package) to the native pixel scales of the wide-field (2001; 0''.1 pix⁻¹) and planetary (2009; 0''.045 pix⁻¹) chips. In order to compare the 2001 and 2009 epochs directly, we also drizzle-combined the latter to the 2001 WF2 resolution of 0''.1 pix⁻¹. Field stars, common to all of the frames, were then used to compute the geometric transforms necessary to register all of the images to better than 0.1 pixel rms.

For the polarimetric analysis of the surrounding compact dust nebula, we manually registered the four individual images using cross-correlation, median combination, and sky subtraction. The final stacks for each polarization angle were geometrically registered to a common reference frame in the same manner as for the narrow-band images. The Stokes parameters U , Q , and I were then computed from linear combinations of three polarization-angle images at a time, as outlined using the online WFPC2 Polarization Calibration Tool¹². To increase the signal-to-noise ratio, at the expense of some resolution, we block-averaged the images by a factor of two, computed Stokes-parameter images for all four permutations of the polarization images, and averaged the resulting data to produce final Stokes images. From these, we calculated the degree of linear polarization and the position angle of the electric vector at each pixel.

To verify our procedure, we also determined P for several unsaturated field stars in the neighborhood of the nebula. They indeed have negligible values of P , as expected since interstellar polarization is almost always quite small. Propagating the Poisson and read-noise errors associated with each individual frame, and the variance of the individual Stokes images, we find these detections of polarization significant at roughly a 2 σ level. While there is some indication that the nebula may have significant levels of linear polarization, the signal-to-noise ratio of these data is too low for further analysis.

2.2. Infrared Photometry

The spectral energy distribution (SED) of V605 Aql shows that there is significant dust around the star emitting in the mid- to far-IR. The SED is plotted in Figure 2. The data, summarized in Table 2, consist of JHK photometry (Hinkle et al. 2008), as well as photometry from the *Infrared Astronomy Satellite (IRAS)* (Walker 1985; Rao & Nandy 1986); the *AKARI* In-

¹¹ IRAF is distributed by the National Optical Astronomy Observatories, which are operated by the Association of Universities for Research in Astronomy, Inc., under cooperative agreement with the National Science Foundation. The Space Telescope Science Data Analysis System (STSDAS) is distributed by the Space Telescope Science Institute.

¹² http://www.stsci.edu/hst/wfpc2/software/wfpc2_pol_calib.html

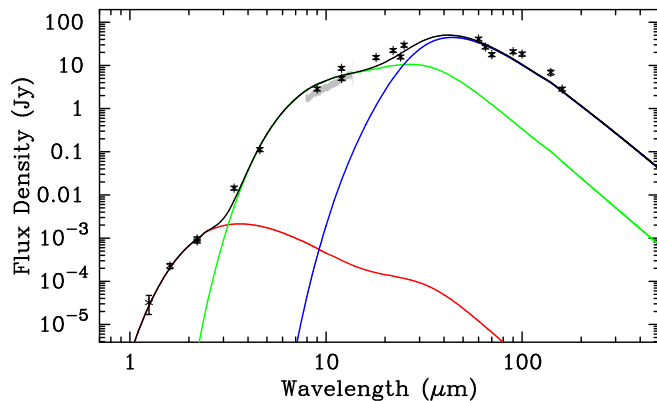


FIG. 2.— The SED of V605 Aql is plotted including *JHK* photometry (Hinkle et al. 2008), and photometry from *IRAS*, *AKARI*, *WISE*, and *Spitzer*/MIPS. The data are listed in Table 2. The grey line is a spectrum obtained with MIDI/VLTI. A three component fit has been done to the points using amorphous carbon dust and three temperatures, 810 K (red), 235 K (green), and 75 K (blue). The sum of three components is shown as a black line.

TABLE 2
V605 AQL PHOTOMETRY

Band	Flux (Jy)
<i>J</i> ^a	3.21e-05 ± 1.5e-05
<i>H</i> ^a	2.27e-04 ± 3.0e-05
<i>K</i> ^a	8.56e-04 ± 8.0e-05
<i>IRAS</i> /12	4.99e+00 ± 2.0e-01
<i>IRAS</i> /25	2.95e+01 ± 1.18e+00
<i>IRAS</i> /60	4.07e+01 ± 4.1e+00
<i>IRAS</i> /100	1.83e+01 ± 2.0e+00
<i>AKARI</i> /9	2.85e+00 ± 1.68e-02
<i>AKARI</i> /18	1.53e+01 ± 1.20e-01
<i>AKARI</i> /65	2.67e+01 ± 2.50e+00
<i>AKARI</i> /90	2.08e+01 ± 9.87e-01
<i>AKARI</i> /140	6.88e+00 ± 9.03e-01
<i>WISE</i> /3.4	1.44e-02 ± 3.05e-04
<i>WISE</i> /4.6	1.13e-01 ± 2.07e-03
<i>WISE</i> /12	8.56e+00 ± 5.52e-02
<i>WISE</i> /22	2.22e+01 ± 1.02e-01
<i>MIPS</i> /24	1.57e+01 ± 8.01e-02
<i>MIPS</i> /70	1.78e+01 ± 1.85e-01
<i>MIPS</i> /160	2.82e+00 ± 1.12e-01

^a *JHK* photometry from Hinkle et al. (2008).

frared Camera (IRC) and Far-Infrared Surveyor (FIS) (Murakami et al. 2007; Ishihara et al. 2010); the *Wide-field Infrared Survey Explorer (WISE)* (Wright et al. 2010); and the *Spitzer* Multiband Imaging Photometer for *Spitzer* (MIPS) (Rieke et al. 2004). MIPS scans at 24, 70, and 160 μm of V605 Aql were downloaded from the archive and photometry was done using PSF-fitting in Starfinder. The other IR Photometry of V605 Aql was collected from the literature and from Vizier.

2.3. MIDI/VLTI

Very Large Telescope Interferometric (VLTI) observations were obtained of V605 Aql at the European Southern Observatory at Paranal in 2007 July using the Mid-infrared Interferometric instrument (MIDI). The first night used the UT2–UT3 baseline, and the second night used the UT4–UT3 baseline, but the source was apparently too large to generate fringes. **This instrument is sensitive to structures with milliarcsecond sizes.**

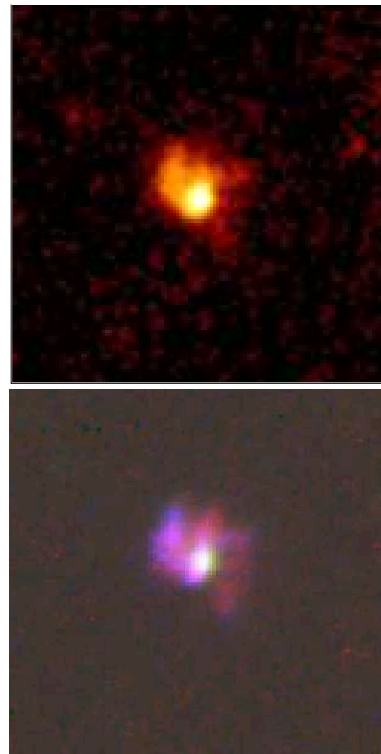


FIG. 3.— Images of V605 Aql. *Top*: Deep *HST* image of in the F547M filter, obtained in 2009 (WFPC2/WF2). This bandpass is dominated by the C IV Wolf-Rayet emission feature in the spectrum of the central star. The image displays a bright, slightly extended “hot spot,” which we interpret as the central star, seen through significant dust extinction. *Bottom*: False-color rendition of the 2009 *HST* images. Red is the nebular [N II] emission line, green is the stellar C IV feature, and blue is the nebular [O III] emission line. The putative central star, represented by the bright white spot, lies near the geometric center of the nebula. North is at the top, east on the left. Each panel is $5'' \times 5''$.

Therefore, these data do not constrain the much larger structures detected elsewhere in this paper. The MIDI spectrum of V605 Aql is shown in Figure 2. The photometric uncertainties are about 20%. The spectrum is featureless, and at a similar flux level to a spectrum obtained with the Infrared Space Observatory (ISO), more than 10 years previously.

3. DIRECT DETECTION OF THE CENTRAL STAR

In Figure 3 (top panel), we show the sum of the four polarimetric *HST* images, taken in the intermediate-width F547M filter, which includes the strong stellar-wind C IV emission feature. This is a very deep image, combining 6 *HST* orbits of imaging. Figure 3 is dominated by a slightly non-stellar “hot spot.” The FWHM of this bright feature is $0''.33$, as compared to $0''.18$ for nearby stars in the field. We suggest that this is the central star itself, but still seen through substantial extinction. The surrounding nebula is much fainter; in this filter the nebula is mostly starlight scattered off dust plus a small amount of [O III] 5007 \AA emission leaking in from the short-wavelength tail of the F547M bandpass.

To illustrate the spatial relationships between the different features, we show in Figure 3 (bottom panel) a false-color image made by registering and combining the [O III], F547M, and [N II] frames from 2009. This image

demonstrates that our putative central star lies near the geometric center of the compact nebula, including the faint extension to the southwest. Note that the near-IR *JHK* images presented by Hinkle et al. (2008) show the same nearly stellar hot spot, which they argued is the central star.

Three of the four polarimetric F547M images were summed by combining the various polarization angles into a Stokes *I* image using linear combinations given by Biretta & McMaster (1997). A “standard” star was chosen in the field which is listed in the GSC2.2 and UCAC4 catalogs as $V = 15.57$, and in NOMAD at 15.4. We assumed a magnitude of $V = 15.5$ for the standard star. Photometry was done on this star and the central star of V605 Aql in the F547M image, using standard techniques in DAOPHOT and psf-fitting. We estimate that the V605 Aql central star is $V = 20.2 \pm 1.0$. The uncertainty is an estimate based on the quality of the profile fitting and the uncertainty in the standard star’s magnitude, but does not try to estimate uncertainties introduced by using a medium-pass filter with no color information. If the the reddening estimate from §5 is used, then the intrinsic apparent brightness of V605 Aql in 2009 was $V = 20.2 - 4 \sim 16.2$. The F547M bandpass is dominated by the C IV Wolf-Rayet emission feature in the spectrum of the central star (Clayton et al. 2006). Therefore, we cannot use the photometry in this filter as an apparent stellar *V* magnitude which could be used with the estimated distance to calculate M_V .

4. MORPHOLOGY OF THE COMPACT NEBULA

Figure 4 shows the [O III] images at the 1991, 2001, and 2009 epochs, and the [N II] images from 2001 and 2009. The brighter portions of the compact nebula in 2009 have an angular diameter of $\sim 1''$; the total diameter is about $1''.7$ if we include the faint extensions on the southwest side. Clayton et al. (2006) suggested that V605 Aql may be surrounded by a thick torus of dust with some stellar light scattering toward the observer from the poles of the torus. This idea was discussed in detail by Hinkle et al. (2008), based on their 2001 *HST* and ground-based images. This model was suggested by the earlier epochs of imaging which showed two blobs of emission separated by a dark band, thought to be an almost edge-on thick disk of dust obscuring the central star in the visible. Guerrero & Manchado (1996) first noted the asymmetry of the central knot, and the dark band was already seen in the aberrated FOC images from 1991 (Figure 4, top left panel), and then more clearly in the deconvolved versions presented by Bond & Pollacco (2002). Hinkle et al. (2008) suggested that the central star was visible in their near-IR imaging and that the disk was inclined enough to see the star in the center of the disk. This morphology is suggestive of a bipolar structure possibly with a central disk. The orientation of the dark band (PA $\sim 150^\circ$) is also approximately parallel to the direction of the major-axis of the surrounding PN, as shown in Figure 1.

Another interpretation of the morphology is that the northeast and southwest emission is coming from material expanding away from the star and its torus or disk at the center. This geometry is shown in Figure 5. It is possible that the dust obscuration of the V605 Aql central star and the nebula is decreasing with time so that

in the latest 2009 imaging, the central star is visible for the first time and the southwest component is seen more clearly. The northeast component is on the near side and less obscured than the southwest component which is on the far side of the star. There is a gradient in the ratio of [O III] to [N II] in the nebula, in the sense that the ratio is highest on the northeast side and lowest on the southwest. This could represent a range in dust extinction, lower on the northeast, near-side, and higher on the southwest, far-side of the star. The gradient could also be due to a range in excitation level.

5. EMISSION-LINE SPECTRAL MODELING

High-resolution (0.35 \AA) spectra of the integrated light of the compact nebula were obtained in mid-1991 by Pollacco et al. (1992), using the coudé echelle spectrograph on the Anglo-Australian Telescope. These spectra showed a system of broad and narrow emission-line components in [O III] and [N II], as well as $H\alpha$ from the surrounding PN, Abell 58. Unfortunately, the original data have now been lost (D. Pollacco, private communication), so we reconstructed them by digitizing the figures in the online version of the journal article and converting them to tables of intensity vs. wavelength.

Pollacco et al. (1992) noted that $H\alpha$ and [N II] 6548–6583 \AA have narrow emission-line components with double profiles. For some unknown reason, the [O III] lines are not split. Attributing these components to the surrounding PN, they derived an expansion velocity of $31 \pm 4 \text{ km s}^{-1}$ and a systemic velocity for the large PN of $+70 \text{ km s}^{-1}$. The spectra also showed much broader emission features in [N II] and [O III] (but not in $H\alpha$), attributed to the compact hydrogen-deficient nebula. The peaks of the broad features were blueshifted by $\sim 100 \text{ km s}^{-1}$ with respect to the systemic velocity, and with FWHMs of 180 and 270 km s^{-1} , respectively. Pollacco et al. interpreted these blueshifted features as arising either from a one-sided collimated flow, or more probably from a dusty, approximately spherical wind, in which the receding (i.e., redshifted) material is obscured by dust within the wind. The latter scenario is bolstered by a subtle indication of a red tail in the broad components, and is the one that we adopt here.

We use a simple model of a spherical nebula of uniform density with radius R , expanding at a constant speed v_{exp} , and a spherical r, θ coordinate system, where θ is the angle relative to the line of sight. A volume element located at (r, θ) will have radial velocity $v_r = -v_{\text{exp}} \cos \theta$. If the optical depth to the center of the sphere is τ , the intensity from that volume element will be extinguished by $\exp(-\tau[Z/R])$, where $Z = \sqrt{R^2 - (r \sin \theta)^2} - r \cos \theta$ is the line-of-sight distance out of the nebula from the volume element toward the observer.

In this model, the emission-line profile, $I(v_r)$, is an integral of extinguished emission over the entire sphere. An asymmetric profile can thus be fit to the observed spectra using standard Levenburg-Marquardt minimization (Press et al. 1992) of the numeric integral as a function of systemic velocity, line width, and the optical depth to the nebula center, τ . We performed such fits on the [O III] 5007 \AA and [N II] 6548–6583 \AA line complexes, as shown in Figure 6. The doubled narrow components were forced to have no internal extinction, as they repre-

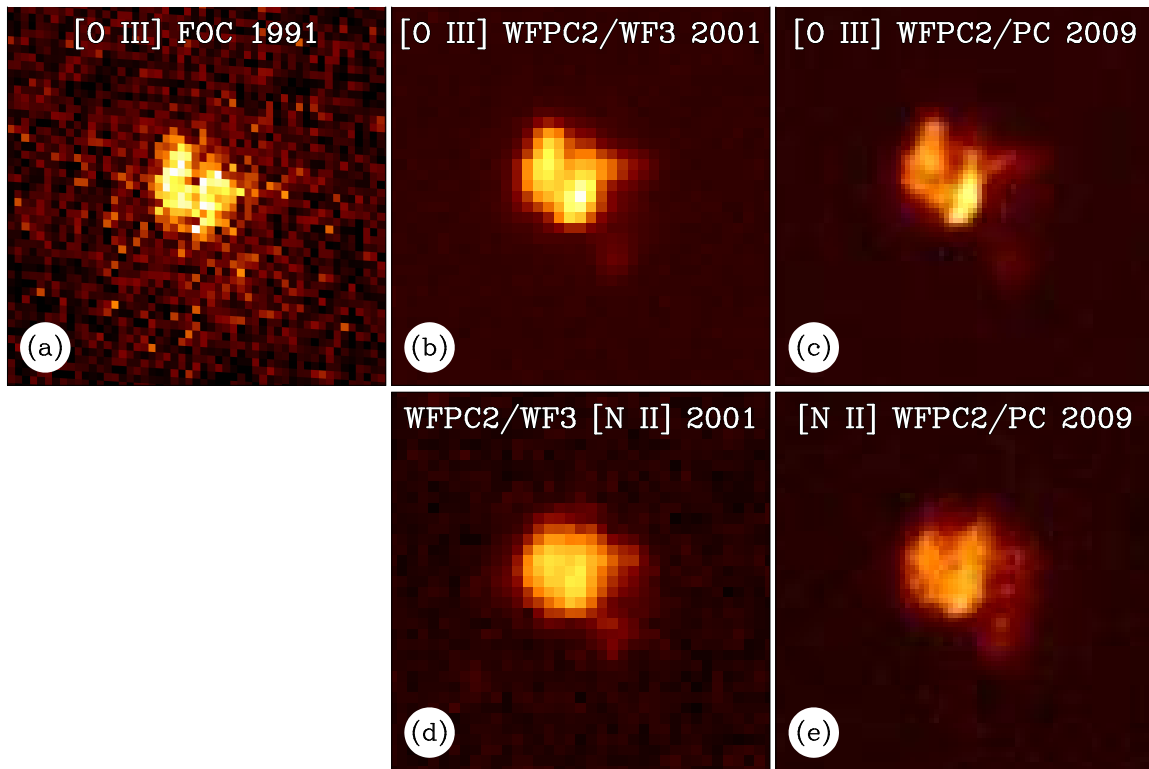


FIG. 4.— Top: *HST* images of the V605 Aql compact nebula in [O III] 5007 Å obtained in (a) 1991 (aberrated FOC), (b) 2001 (WFPC2/WF3), and (c) 2009 (WFPC2/PC). Linear stretches were used. Bottom: *HST* images of V605 Aql in [N II] 6583 Å obtained in (d) 2001 (WFPC2/WF3) and (e) 2009 (WFPC2/PC). Note expansion of the nebula from 2001 to 2009. Each panel is $5'' \times 5''$. North is at the top, east on the left in all images.

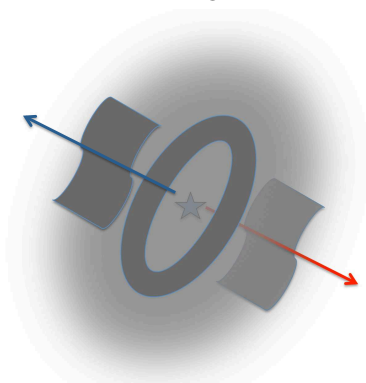


FIG. 5.— Cartoon showing the central star of V605 Aql at the center of a tilted torus with the material in the northeast (upper left) expanding away on the near side, and the material in the southwest (lower right) expanding away on the far side. The material on the far side experiences more dust extinction and so appears fainter.

sent emission from the outer PN, Abell 58. The narrow lines yield a mean systemic velocity of $+80 \text{ km s}^{-1}$, very close to that found by Pollacco et al. (1992) from these spectra. The best fit model is also shown in Figure 6.

No single asymmetric profile can account for all of the broad emission; however, we find that the bulk of the emission, including the broad red and blue tails, can be well fit by a single sphere at a systemic velocity of $+80 \text{ km s}^{-1}$, and an expansion velocity of 215 km s^{-1} , with $\tau = 4.0$ for [O III] and 3.0 for [N II]. These components of the line profiles are shown in green in Figure 6. The ratio of optical depths is that expected for

pure carbon dust following a Mathis et al. (1977, hereafter MRN) grain-size distribution, and corresponds to an extinction toward the central star of $A_V = 4 \text{ mag}$. Note that this model does not account for profile broadening due to thermal motions, slit width and the line-spread function of the optical system. To fully reproduce the observed profile, we would have to add or subtract some narrow features, which suggests that the outflow has clumpy substructure, consistent with the narrow-line images presented in Figure 4. The Galactic latitude of V605 Aql is -5° which implies a foreground interstellar extinction of $A_V \sim 1.45 - 1.75 \text{ mag}$ (Schlegel et al. 1998; Schlafly & Finkbeiner 2011). So the total extinction toward V605 Aql is $\sim 5.5 \text{ mag}$. The uncertainty in this estimate is substantial as the extinction estimates from both the emission line fits and the foreground component contain simplifying assumptions.

6. ANGULAR EXPANSION

A primary goal of this investigation was to measure the angular expansion of the compact nebula. Visual inspection of the [O III] and [N II] images in Figure 4 does confirm noticeable expansion.

We chose the [O III] images from 2001 and 2009 (separated by 7.8 years) for detailed analysis. As described in §2, we resampled the 2009 image to the (lower) resolution of the 2001 image. We then magnified the earlier image by various factors and subtracted it from the later one, and sought to minimize the residual fluxes. Figure 7 shows PSF-matched difference images for magnifications of 0%, 8%, and 16% between the 2001 and 2009 epochs.

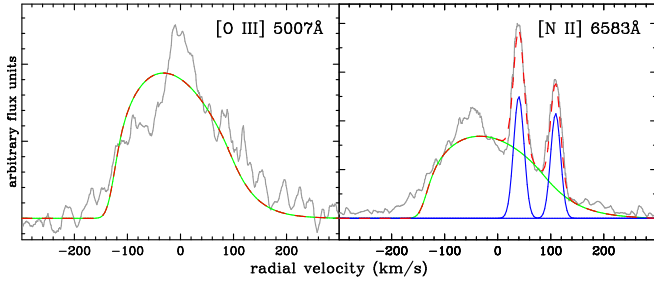


FIG. 6.— Model fits to the V605 Aql emission-line spectra of [O III] 5007 Å and [N II] 6583 Å. *Grey lines*: observed spectra from Pollacco et al. (1992). *Blue profiles*: [N II] components attributed to the surrounding planetary nebula Abell 58, with center-of-mass velocity of $+75 \text{ km s}^{-1}$. *Green lines*: single-line profile fits using a uniform-density spherical nebula with a dust extinction of $A_V = 4$ to the center; these yield an expansion velocity $v_{\text{exp}} = 220 \text{ km s}^{-1}$ relative to center of mass. *Dashed red lines*: sum of model components.

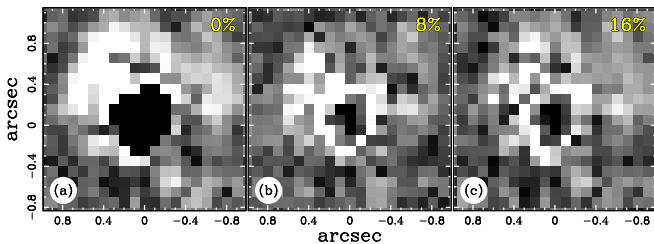


FIG. 7.— Difference images between the WFPC2 F502N data from 2001 and 2009, with the former epoch magnified by the scaling shown in each panel. White is positive and black is negative. The images are centered on the star. (a) Difference image with no magnification, showing result of simple PSF-matching and flux-scaled subtraction. (b) Difference with 8% magnification, yielding smallest sum of residuals. (c) Difference with 16% magnification. Absolute residuals are ~ 5 times larger than for best-fit magnification of 8%.

The 0% and 16% difference have much larger residuals due to the expansion of the nebula, and the 8% image is the best fit.

The magnification residuals were minimized as follows. Assuming a homologous expansion by a magnification factor a , and denoting the reference and input images by R and I , and the magnified input image by aI , we calculate the sum of the squared residuals, $\rho(a) = \sum_{\text{pix}} (R - aI)^2$. The most likely expansion factor is then the value a_{min} that minimizes ρ .

The uncertainty can be directly computed as $\sigma = \sqrt{\langle a^2 \rangle - \langle a \rangle^2}$, where $\langle x \rangle$ is the expectation value of the parameter x , i.e., $\langle a \rangle = \int a \rho(a) da$, if ρ has been normalized. When nebulae are better resolved, one can perform this task across various wedges or quadrants in position angle, in order to determine the local average expansion, or one can compare the expansion of individual features to measure the microscopic expansion properties (Li et al. 2002; Ueta et al. 2006). However, since the V605 Aql nebula is only marginally resolved, we opted for a global measurement in which the entire nebula is assumed to expand homologously.

As a note of caution, when the input and reference images have PSFs that differ significantly, the residual ρ may not be minimized for the actual best-fit magnification factor, even if that factor is exactly known ahead of time. We attempted to minimize this problem by PSF-matching the WFPC2 images before computing the dif-

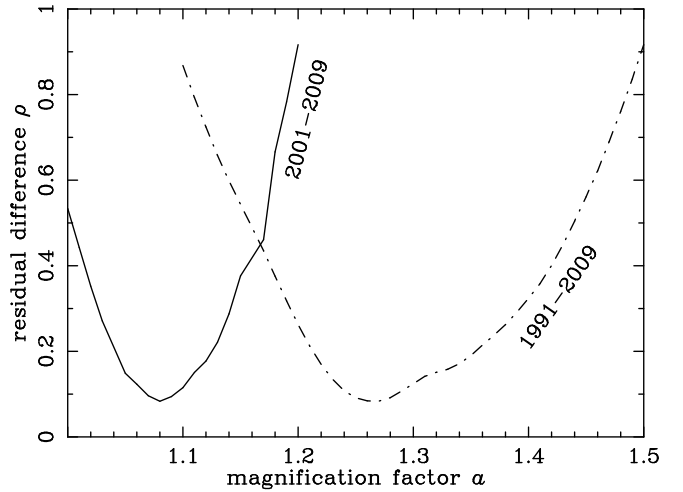


FIG. 8.— Normalized residual differences $\rho(a)$ vs. magnification factor a for the WFPC2 F501N images from 2001 and 2009 (*solid line*) and the deconvolved 1991 F501N FOC and 2009 F502N WFPC2 images (*dot-dashed line*). The best-fit expansion of the nebula between the two epochs is the minimum of each curve.

ference residuals, and by masking out pixels surrounding the bright, quasi-stellar source at the center of the nebula.

Figure 8 plots the normalized residuals for the [O III] filter against magnification factor, for the 2001-2009 pair (*solid line*) and the 1991-2009 pair (*dot-dash line*). For the 2001-2009 WFPC2 images, the derived expansion factor is $8 \pm 2\%$. We verified this numerical result in a “double-blind” fashion, by visually examining residual images produced by scaling and subtracting the two epochs, and selecting the magnification factors that appeared best, without knowledge of the results plotted in Figure 8. The flattest-appearing residuals were indeed close to the 8% value. Not shown here is a similar exercise for the 2001-2009 [N II] images, which gave an expansion factor of $5 \pm 3\%$.

Under the assumption of homologous expansion, the 2001-2009 [O III] data yield an ejection epoch of 1903 ± 49 . Performing the same exercise between the the 2009 WFPC2 image and the FOC data from 1991 yields an expansion factor of $27 \pm 9\%$, as shown in Figure 8, and an ejection epoch of 1926 ± 22 . Both results are thus consistent, within the errors, with an ejection of the compact nebula at the time of the 1919 optical outburst.

7. GEOMETRIC DISTANCE

We estimated the distance to V605 Aql using the expansion-parallax method. In this technique, the distance is determined by equating the velocity implied by the angular expansion rate in the plane of the sky, derived in the previous two sections, to the expansion velocity in the line of sight.

In order to estimate a distance to V605 Aql based on the expansion parallax, we need to convert the fractional expansion rate of the compact nebula into angular units. We measured this by considering each of the four quadrants of the image, and determining the radial pixel shift needed to match features between epochs. We found that a radial shift of $0''.08 \pm 0''.01$ minimizes the subtraction residuals.

We also used a “by-eye” approach, in which we estimated the location of the outer edge of the nebula

from high-contrast renditions of the images. This visual method also yielded an estimated expansion of $0''.08$ over the 7.8-year epoch difference. The angular expansion rate is thus $10.2 \pm 1.3 \text{ mas yr}^{-1}$.

A rough geometric distance, d , can be estimated from the observed angular radius, $a \simeq 0''.85$ at epoch $t = 2009$, as discussed in §4, combined with the expansion velocity of $v_{\text{exp}} = 215 \pm 20 \text{ km s}^{-1}$. We assume a simple spherical expansion (in spite of the obviously non-spherical appearance of the compact nebula), and that it was ejected in 1919. The result is

$$d \simeq 4.8 \text{ kpc} \left(\frac{0''.85}{a} \right) \left(\frac{v_{\text{exp}}}{215 \text{ km s}^{-1}} \right) \left(\frac{t - 1919}{2009 - 1919} \right),$$

but this is somewhat uncertain, since the nebular radius is poorly defined.

An alternative calculation, using instead the angular expansion rate of $\theta = 10.2 \pm 1.3 \text{ mas yr}^{-1}$, yields

$$d \simeq 4.4 \text{ kpc} \left(\frac{v_{\text{exp}}}{215 \text{ km s}^{-1}} \right) \left(\frac{10.2 \text{ mas yr}^{-1}}{\theta} \right),$$

with a formal error of about $\pm 0.6 \text{ kpc}$. There is likely a significant systematic error because of our assumption of a simple spherical expansion. The images of the V605 Aql knot clearly show that it is not spherical so the expansion velocity in the plane of the sky may be larger than in the radial direction, in which case our distance estimates would be too low.

Other distance estimates, based on various methods applied to the large PN Abell 58, have been reviewed by Clayton & De Marco (1997) and Hinkle et al. (2008), and range from 2.7 to about 6 kpc. The result estimated here, $\sim 4.6 \text{ kpc}$, is consistent with the previous estimates, given the large uncertainties and systematic errors in all of the methods.

8. DUST MASS

Koller & Kimeswenger (2001) modeled the dust emission from V605 Aql using a radiative transfer code which fit *Infrared Space Observatory* (ISO) and *IRAS* photometry of the star. They assumed that $d = 5 \text{ kpc}$, $T_{\text{eff}} = 100,000 \text{ K}$, and $L_{\star} = 5800 L_{\odot}$. They also assumed carbon dust with $A_V = 7$ and found a dust mass of $8 \times 10^{-3} M_{\odot}$. Hinkle et al. (2008) fit IR photometry from the J-band to $14.5 \mu\text{m}$ with two dust components emitting as blackbodies with temperatures of 350 and 1500 K, but don't estimate the total dust mass.

Wesson et al. (2008) calculated a gas mass for the ejected knot of $5 \times 10^{-5} M_{\odot}$ assuming a distance of 3.5 kpc, $n_e = 2100 \text{ cm}^{-3}$, and an angular radius of $0''.38$. The angular radius corresponds to $2 \times 10^{16} \text{ cm}$ at 3.5 kpc. This agrees well with the size of a nebula expanding at 215 km s^{-1} for 90 yr ($6 \times 10^{16} \text{ cm}$). They estimate the extinction from $c(\text{H}\beta) = 2.0$ for the inner knot which corresponds to $A_V \sim 3 \text{ mag}$.

The SED of V605 Aql, shown in Figure 2, was fit using various dust components at different temperatures. As described in Sugerman et al. (2012), a zeroth-order estimate of the emitting dust mass can be produced by fits to the observed SED. Each dust component has a single temperature, and emits as a blackbody modified by

the mass-absorption coefficient. In addition, each was assumed to be optically thin, 100% amorphous carbon with an MRN distribution, and optical constants from Weingartner & Draine (2001). Figure 2 shows the best fit which required dust with three different temperatures and masses (810 K, $1 \times 10^{-11} M_{\odot}$; 235 K, $9 \times 10^{-6} M_{\odot}$; 75 K, $2 \times 10^{-3} M_{\odot}$). There is a range of models that fit the data roughly equivalently, with masses that are consistent to within a factor of two of those presented here. Also, these dust masses are lower limits to the values one would find when running a Monte-Carlo radiative-transfer model.

We have estimated in §5 that V605 Aql suffers from ~ 4 mag of internal extinction at V. Let's assume a spherical shell of dust with a radius of $2 \times 10^{16} \text{ cm}$ around the star as did Wesson et al. (2008). Then, looking through the dust to the star, the optical depth is, $\tau = \kappa \rho L$, where ρ is the dust mass density, κ is the mass absorption coefficient, and L is the path length. V605 Aql is carbon rich (Clayton et al. 2006), and the *Spitzer*/IRS spectrum shows no silicate or PAH features so the dust is likely to be amorphous carbon (Evans et al. 2006). A typical value for the absorption coefficient is $\kappa \sim 5 \times 10^5 \text{ cm}^2 \text{ g}^{-1}$ (Zubko et al. 1996; Draine & Li 2007). If $L = 2 \times 10^{16} \text{ cm}$ and $\tau = 4$, then $\rho = 4 \times 10^{-22} \text{ cm}^2 \text{ g}^{-1}$. Then, the mass of dust in the shell is just $4/3 \pi L^3 \rho$ or $\sim 7 \times 10^{-6} M_{\odot}$.

This implies a gas-to-dust ratio of ~ 7 which is very small compared to the typical gas-to-dust-ratio for the Galaxy of 100 (Draine et al. 2007). However, the gas-phase abundances in the central knot of V605 Aql are very different than those seen in a typical interstellar cloud. Wesson et al. (2008) measured the fractional abundances of various elements in the V605 knot, H (0.019), He (0.250), C (0.021), N (0.043), O (0.323), and Ne (0.345). Firstly, H, which is typically 75% of interstellar gas, and does not deplete into dust grains, is missing, which will lower the gas-to-dust ratio significantly. Among the other abundant elements in the central knot, Ne and He will also be undepleted as they do not participate in the grain chemistry. In the ISM, C and O are heavily depleted into carbon grains and silicate grains. However, the MIDI, ISO, and *Spitzer* Infrared Spectrograph (IRS) (Evans et al. 2006) observations of V605 Aql indicate that its mid-IR spectrum is a featureless continuum. This is similar to what is seen in the RCB stars (Kraemer et al. 2005). There are no silicate features at 10 and $20 \mu\text{m}$, and no sign of PAHs or SiC. The featureless spectrum indicates that the dust around V605 is probably amorphous carbon, i.e., 100% carbon. So, it is likely that carbon is highly depleted into grains, but that the other elements, measured by Wesson et al. (2008), are not. If carbon is depleted at a level that we see in the ISM, then probably 90% of the carbon is in dust. In the gas phase in the V605 knot, carbon is $\sim 1 \times 10^{-6} M_{\odot}$. If carbon is 90% depleted, then the total mass of carbon (gas phase and in dust) in the knot is $1 \times 10^{-5} M_{\odot}$. Then the gas-to-dust ratio is ~ 5 , which is remarkably low. This estimate for the dust mass ($1 \times 10^{-5} M_{\odot}$) fits in very well with the estimates above from the extinction and likely size of the shell ($7 \times 10^{-6} M_{\odot}$), and from the hot and warm dust components of the SED fit ($9 \times 10^{-6} M_{\odot}$).

Assuming that the mass of C is actually $1 \times 10^{-5} M_{\odot}$,

increases the mass of the central knot to $5.9 \times 10^{-5} M_{\odot}$, and changes the ratio C/O from 0.06 to 0.6 but still well below unity and far below the large C/O predicted for a FF.

Wesson’s estimate of the gas mass measures only hot gas near the star. The second of the mass estimates in Wesson et al. (2008) used a density of 2100 cm^{-3} , derived from collisionally excited lines, so that could underestimate the gas mass if there were regions of very high density to quench the CEL emission. Also, the apertures for the near- and mid-IR photometry, plotted in Figure 2, have sizes of a few arcseconds and are measuring the hot gas and dust in the central knot. But, the apertures for the far-IR ($>20 \mu\text{m}$) photometry are much larger, *IRAS* (spatial resolution $\sim 4'$) and *AKARI/FIS* (spatial resolution $\sim 35''$), and may be including colder dust further from the star, possibly associated with the PN which is $44'' \times 35''$ in size (Abell 1966). This idea is supported by the fact that the flux density in the *Spitzer/MIPS* images, which have a better spatial resolution, is slightly lower. So, the value estimated above, $\sim 1 \times 10^{-5} M_{\odot}$, is probably consistent with the dust mass in the central knot. The large mass of cold dust, $2 \times 10^{-3} M_{\odot}$, estimated from the SED fit, likely lies outside the knot. A significant mass of cold dust was also recently found around R CrB, which is a possible FF star (Clayton et al. 2011).

9. SUMMARY

New polarimetric imaging with *HST*/WFPC2 in nebular [O III], [N II] and stellar C IV provides a baseline of 18 years to investigate the expansion of the ejecta from the 1919 event, and allow us to investigate the position and extinction of the central star. The new measurements of the rate of the expansion, reported here, are consistent with an ejection in 1919. When combined with velocities measured from spectra of V605 Aql, a distance of 4.6 kpc is estimated, which is in the middle of the range of previous distance estimates.

The morphology of the 1919 ejecta is highly non-spherical. It seems to be either a tilted dusty torus with a dark band, or a disk surrounding the central star with bipolar ejections on either side. Further imaging as the expansion continues may clarify this. The asymmetry of the knot is aligned with the asymmetry of the much larger surrounding PN. A disk and PN asymmetry could result if V605 Aql is a binary system (Lau et al. 2011). There is early evidence that there is a disk around Sakurai’s Object (Chesneau et al. 2009).

The new *HST* images of V605 Aql, presented here, provide the first direct detection of the central star in the visible since 1923. In the stacked F547M image, the star is $V = 20.2 \pm 1.0$ mag. We estimate that the intrinsic apparent magnitude today should be $V \sim 16.2$ mag, assuming the extinction is $A_V \sim 4$ mag which is estimated from the spectral modeling. This modeling estimates a systemic velocity of $+80 \text{ km s}^{-1}$ and an ex-

pansion velocity of 215 km s^{-1} . Polarimetric imaging was obtained to investigate whether the 2001 spectrum of V605 Aql (Clayton et al. 2006) was obtained primarily in scattered light from dust in the central knot, but the signal-to-noise in the data was not sufficient to measure the level of polarization.

It is found that the SED of the dust around V605 Aql, consisting of Near-IR, IRAS, WISE, AKARI, and Spitzer photometry, can be fit using carbon dust with three different temperatures and masses. Using three different methods, we estimate a mass of warm dust in the central knot of $\sim 10^{-5} M_{\odot}$. A significant mass of cold dust ($10^{-3} M_{\odot}$) may be spread over a larger volume perhaps associated with the surrounding PN.

V605 Aql is one of only three stars, identified with a final helium-shell flash, to be observed from their initial brightening. It is very similar to the more recent FF star, Sakurai’s Object. Monitoring of V605 Aql is important because it may allow the future behavior of Sakurai’s Object to be predicted and better observed. In V605 Aql, the composition of the hydrogen-deficient ejecta (the C/O ratio below unity and a Ne mass fraction of 35%), however, leaves little doubt that the scenario that formed this object is far more complex than a FF (that predicts C/O far larger than unity and a Ne mass fraction of 2% (Werner & Herwig 2006)). V605 Aql must have passed through a phase involving the dredge-up of Ne from the core of an ONe WD. Another object currently listed in the FF class, Abell 30, also has hydrogen-deficient knots with similar abundance trends (C/O below unity and a Ne mass fraction between 8 and 20% (Wesson et al. 2003)). The ONe nova scenario, proposed by Lau et al. (2011) to explain these abundance patterns, may not be viable because it does not include the compulsory series of carbon-oxygen nova outbursts that precede the ONe nova detonation. If so, then the only viable scenario is that of a merger between a massive ONe white dwarf and a companion. At the present time, it is not possible to resolve whether V605 Aql is the result of a final helium-shell flash, an ONe nova, or a merger event.

We thank the anonymous referee for several helpful suggestions. Support for this work was provided by NASA through grant number HST-GO-11985 from the Space Telescope Science Institute, which is operated by AURA, Inc., under NASA contract NAS 5-26555; and by the Goucher College Office of the Provost. Some of the data presented in this paper were obtained from the Mikulski Archive for Space Telescopes (MAST). We would like to acknowledge James Liebert, Alvio Renzini, and Nye Evans for assisting with this work. This research has made use of the VizieR catalogue access tool, CDS, Strasbourg, France.

Facilities: HST (WFPC2, FOS, FOC)

REFERENCES

- Abell, G. O. 1966, ApJ, 144, 259
 Bailey, S. I. 1921, Harvard College Observatory Bulletin, 753, 2
 Bidelman, W. P. 1971, ApJ, 165, L7
 Bidelman, W. P. 1973, in Bulletin of the American Astronomical Society, Vol. 5, Bulletin of the American Astronomical Society, 442
 Biretta, J., & McMaster, M. 1997, WFPC2 Polarization Calibration, Tech. rep.

- Biretta, J., & Sparks, W. 1995, WFPC2 Polarization Observations: Strategies, Apertures, and Calibration Plans, Tech. rep.
- Bond, H. E., Liebert, J. W., Renzini, A., & Meakes, M. G. 1992, in European Southern Observatory Conference and Workshop Proceedings, Vol. 44, European Southern Observatory Conference and Workshop Proceedings, ed. P. Benvenuti & E. Schreier, 139
- Bond, H. E., Meakes, M. G., Liebert, J. W., & Renzini, A. 1993, in IAU Symposium, Vol. 155, Planetary Nebulae, ed. R. Weinberger & A. Acker, 499
- Bond, H. E., & Pollacco, D. L. 2002, *Ap&SS*, 279, 31
- Cannon, A. J., & Pickering, E. C. 1916, *Annals of Harvard College Observatory*, 76, 19
- Chesneau, O., et al. 2009, *A&A*, 493, L17
- Clayton, G. C. 2012, *JAAVSO*, 40, 539
- Clayton, G. C., & De Marco, O. 1997, *AJ*, 114, 2679
- Clayton, G. C., Kerber, F., Pirzkal, N., De Marco, O., Crowther, P. A., & Fedrow, J. M. 2006, *ApJ*, 646, L69
- Clayton, G. C., et al. 2011, *ApJ*, 743, 44
- Draine, B. T., & Li, A. 2007, *ApJ*, 657, 810
- Draine, B. T., et al. 2007, *ApJ*, 663, 866
- Duerbeck, H. W. 2002, *Ap&SS*, 279, 5
- Evans, A., et al. 2006, *MNRAS*, 373, L75
- Ford, H. C. 1971, *ApJ*, 170, 547
- Fuhrmann, B. 1981, Zentralinstitut fuer Astrophysik Sternwarte Sonneberg Mitteilungen ueber Veraenderliche Sterne, 9, 13
- Guerrero, M. A., & Machado, A. 1996, *ApJ*, 472, 711
- Hajduk et al., M. 2005, *Science*, 308, 231
- Harrison, T. E. 1996, *PASP*, 108, 1112
- Herwig, F. 2001, *ApJ*, 554, L71
- Hinkle, K. H., Lebzelter, T., Joyce, R. R., Ridgway, S., Close, L., Hron, J., & Andre, K. 2008, *A&A*, 479, 817
- Iben, I., Kaler, J. B., Truran, J. W., & Renzini, A. 1983, *ApJ*, 264, 605
- Ishihara, D., et al. 2010, *A&A*, 514, A1
- Kerber, F. 2001, *Ap&SS*, 275, 91
- Kerber, F., Blommaert, J. A. D. L., Groenewegen, M. A. T., Kimeswenger, S., Käufl, H. U., & Asplund, M. 1999, *A&A*, 350, L27
- Kerber, F., Pirzkal, N., De Marco, O., Asplund, M., Clayton, G. C., & Rosa, M. R. 2002, *ApJ*, 581, L39
- Koller, J., & Kimeswenger, S. 2001, *ApJ*, 559, 419
- Kraemer, K. E., Sloan, G. C., Wood, P. R., Price, S. D., & Egan, M. P. 2005, *ApJ*, 631, L147
- Lau, H. H. B., de Marco, O., & Liu, X. 2011, *MNRAS*, 410, 1870
- Lawlor, T. M., & MacDonald, J. 2003, *ApJ*, 583, 913
- Lechner, M. F. M., & Kimeswenger, S. 2004, *A&A*, 426, 145
- Li, J., Harrington, J. P., & Borkowski, K. J. 2002, *AJ*, 123, 2676
- Lundmark, K. 1921, *PASP*, 33, 314
- Mathis, J. S., Rimpl, W., & Nordsieck, K. H. 1977, *ApJ*, 217, 425
- Murakami, H., et al. 2007, *PASJ*, 59, 369
- Pollacco, D. L., Lawson, W. A., Clegg, R. E. S., & Hill, P. W. 1992, *MNRAS*, 257, 33P
- Press, W. H., Teukolsky, S. A., Vetterling, W. T., & Flannery, B. P. 1992, *Numerical recipes in FORTRAN. The art of scientific computing*
- Rao, N. K., & Nandy, K. 1986, *MNRAS*, 222, 357
- Rieke, G. H., et al. 2004, *ApJS*, 154, 25
- Schlafly, E. F., & Finkbeiner, D. P. 2011, *ApJ*, 737, 103
- Schlegel, D. J., Finkbeiner, D. P., & Davis, M. 1998, *ApJ*, 500, 525
- Seitter, W. C. 1985, *Mitteilungen der Astronomischen Gesellschaft Hamburg*, 63, 181
- Sugerman, B. E. K., et al. 2012, *ApJ*, 749, 170
- Ueta, T., Murakawa, K., & Meixner, M. 2006, *ApJ*, 641, 1113
- van den Bergh, S. 1971, *PASP*, 83, 819
- Walker, H. J. 1985, *A&A*, 152, 58
- Weingartner, J. C., & Draine, B. T. 2001, *ApJ*, 548, 296
- Werner, K., & Herwig, F. 2006, *PASP*, 118, 183
- Wesson, R., Barlow, M. J., Liu, X., Storey, P. J., Ercolano, B., & de Marco, O. 2008, *MNRAS*, 383, 1639
- Wesson, R., Liu, X., & Barlow, M. J. 2003, *MNRAS*, 340, 253
- Wolf, M. 1920, *Astronomische Nachrichten*, 211, 119
- Wright, E. L., et al. 2010, *AJ*, 140, 1868
- Zubko, V. G., Mennella, V., Colangeli, L., & Bussoletti, E. 1996, *MNRAS*, 282, 1321